Impact of ion-host interactions on the 5*d*-to-4*f* spectra of lanthanide rare-earth-metal ions. II. The Ce-doped elpasolites

Brian F. Aull* and Hans P. Jenssen
Crystal Physics and Optical Electronics Laboratory, Center for Materials Science and Engineering, Massachusetts Institute of Technology, Cambridge, Massachusetts 02139
(Received 28 March 1986)

Crystal growth of Ce-doped fluoride elpasolites is reported. Single crystals of Rb_2NaYF_6 and Rb_2NaScF_6 have been obtained by both vertical Bridgman and Czochralski techniques. Attempts to grow K_2NaYF_6 by both methods yielded only polycrystalline samples. Ce-doped Rb_2NaYF_6 and K_2NaYF_6 display two distinct emitting centers, one in the blue and another in the near uv. Ce:Rb_2NaScF_6 displays only the blue-emitting center, and Ce:K_2NaScF_6 displays only the uv-emitting center. Growth and spectroscopic investigation of Rb_2NaYF_6 doped with other rare earths established that the blue-emitting center is Ce^{3+} in the normal (Y or Sc) site. The uv-emitting center is Ce^{3+} in a larger, lower-symmetry site. It is hypothesized that this second site is related either to disordering or to the intergrowth of a second phase. Absorption, emission, excitation, and vacuum-uv transmission spectra were measured on Ce-doped elpasolites. Covalent contributions to the crystal field are numerically estimated by comparing the observed 5*d* energy levels with those predicted by an ionic-model calculation. These estimates as well as the qualitative dependence of the 5*d* energies on the lattice constant indicate that covalent contributions to the crystal field are significant. Design rules are suggested for choosing a fluoride host crystal for a visible-wavelength Ce^{3+} laser.

I. INTRODUCTION

In the preceding paper referred to here as paper I,[1] the crystal-field effects determining the 5*d* energy levels of a Ce^{3+} impurity ion in an ionic host crystal were reviewed. A phenomenological model for the dependence of the 5*d* levels on nearest-neighbor distance (or lattice constant) was synthesized. With sufficient data on the 5*d* levels in isostructural hosts, the parameters of the model can be quantitatively determined, or at least approximated from qualitative features of the observed lattice-constant dependence. In this paper we present results on the growth and spectroscopic evaluation of the fluoride elpasolites (A_2NaMF_6; A=Rb or K, M=Y or Sc) doped with cerium and other rare earths.

The elpasolites are an attractive model system for 5*d* crystal-field studies. The rare-earth (RE) site has perfect O_h symmetry and octahedral coordination. For *d* electrons, there is only one nonvanishing crystal-field splitting parameter, and its magnitude falls off rapidly with nearest-neighbor distance (e.g., $1/R^5$ in a point-charge model). This is ideal for studying the contact interactions, such as covalency, which cause departures from the predictions of a purely electrostatic model.

Interest in the Ce^{3+}-doped fluoride elpasolites was first sparked by Chang[2] at Yale University, who measured fluorescence, excitation, and excited-state absorption on polycrystalline samples of Cs_2NaYF_6:Ce. He found broadband blue emission centered at 450 nm, a pump band centered at 310 nm which is compatible with nitrogen-laser and XeCl-laser pumping, and observed optical gain. So the Ce^{3+}-doped fluoride elpasolites showed promise as tunable blue laser materials with low excited state absorption and practical resonant pumping schemes.

The blue emission was unexpected because in other fluorides with Y^{3+} sites, such as $LiYF_4$ and BaY_3F_8, the emission of Ce^{3+} is always observed in the uv near 300 nm. The goal of this research was to measure 5*d* splittings, centroids, and Stokes shifts in the elpasolites in order to test the effect of "site size," and also to make possible a comparison with the lower-symmetry fluorides, and elucidate the physical reasons for the spectroscopic differences.

We have measured the absorption and emission spectra of Ce, and confirmed that the absorption bands are due to Ce by performing excitation measurements. The energy-level positions are determined using a semiclassical approach, that is band centroids in the absorption and transmission spectra are assumed to measure the energies of the purely electronic transitions with the lattice fixed in the equilibrium position. The energy difference between the lowest energy 4*f*-to-5*d* absorption band and the corresponding emission band is the Stokes shift.

K_2NaYF_6 and Rb_2NaYF_6 display two distinct Ce^{3+} emitting centers. Thus much of the experimental work involved identification of the "normal" site.

II. CRYSTAL GROWTH AND X-RAY ANALYSIS

The elpasolite lattice belongs to the space group $Fm3m$ (O_h^5), and Fig. 1 shows one octant of a cubic unit cell of A_2NaMF_6. The Na^+ and M^{3+} ions form a rock salt lattice, and the A^+ ions sit at all equivalent $(\frac{1}{4}, \frac{1}{4}, \frac{1}{4})$ positions. The F^- ions lie between the Na^+ and the M^{3+} ions at some fractional distance, forming regular octahedra around M^{3+} and slightly larger regular octahedra around Na^+. The Na and RE sites have O_h symmetry,

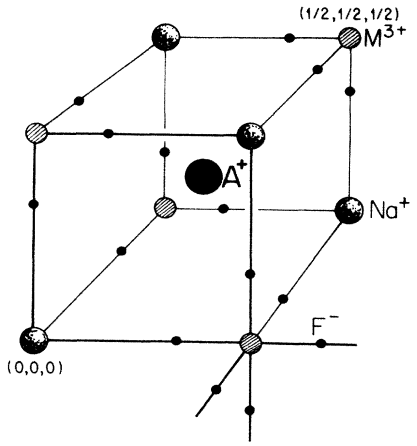

FIG. 1. Elpasolite structure.

the A site has T_d symmetry, and the F site has C_{4v} symmetry.

Since the mid-1950's powders and polycrystalline samples of fluoride elpasolites have been synthesized.[3–11] The first reported growth of large single crystals was by Guggenheim.[12] who grew Rb_2NaMF_6 (M is rare earth or Y) by horizontal zone melting. Subsequent work on the Czochralski growth and x-ray analysis of elpasolites was reported by Gabbe, Aull, and Linz.[13] They found that Rb_2NaYF_6, K_2NaYF_6, and K_2NaScF_6 are incongruently melting compounds.

For this study, Rb_2NaYF_6, K_2NaYF_6, and Rb_2NaScF_6 crystals were grown by the vertical Bridgman technique in a sealed graphite crucible. The starting materials were obtained by hydrofluorination of commercial grade oxides and carbonates. The crucible was evacuated and backfilled with argon or forming gas through a weep hole in the bottom, which was then sealed by a plug of solidified melt. The crucible was heated by an rf-heated graphite susceptor and was lowered out of the hot-zone, typically at 1 mm/h, during the growth run. A further attempt was also made to grow K_2NaYF_6 by Czochralski pulling. More detailed descriptions of the hydrofluorinator, and the Bridgman and Czochralski furnaces are found elsewhere.[14,15]

Single crystals of Rb_2NaYF_6 were successfully grown, doped with Ce, Er, Nd, or La. Consistent with previous results,[12,13] the elpasolite was sandwiched between mixed phase regions at either end of the boule, the boundaries being quite sharp, but mechanically strong and free of cracking. Gabbe's observations during Czochralski growth[13] indicate that the first section to crystallize is a solid solution which decomposes upon cooling. In all the Bridgman growth experiments a Na-enriched feed composition was used (47 mol % RbF, 31 mol % NaF, 22 mol % YF_3), since this had been found by Gabbe to yield less solid solution and more elpasolite than the stoichiometric composition. The mixed phase regions each constituted about a fourth of the length of the boule.

K_2NaYF_6 behaves in a similar fashion. The initial material to crystallize is a solid solution which decomposes upon cooling, and is separated from the elpasolite by a sharp, but mechanically contiguous boundary. However, Bridgman and Czochralski growth experiments on Ce-doped K_2NaYF_6 yielded only polycrystalline samples with many inclusions. During the Czochralski growth experiment it became apparent that constitutional supercooling is a particularly severe problem in this system. A few hours after the elpasolite phase field was entered, the melt at the growth interface broke up into cells, and pulling had to be stopped to allow for remixing of the melt. When pulling was resumed, even at only 0.5 mm/h, the phenomenon reoccurred within two to three hours. Again, when a Na-enriched feed composition was used, the elpasolite phase field was entered after about a fourth of the melt had solidified.

Rb_2NaScF_6 doped with Ce was also grown by the Bridgman technique using a Na-enriched melt composition. Clear single crystalline material was obtained and there was no region of solid solution. Rb_2NaScF_6 may be congruently melting, although a stoichiometric composition has not been tried.

X-ray powder patterns were run on the elpasolites to verify the structure and measure the lattice constant. Table I shows the results, including Gabbe's result on K_2NaScF_6. In the case of K_2NaYF_6, powder patterns were also run on the decomposed solid-solution regions. These patterns showed a diffuse elpasolitelike pattern plus many additional reflections. In the case where a stoichiometric melt was used, these additional reflections were roughly equal in intensity to the "elpasolite" reflections. With the Na-enriched melt, the "elpasolite" reflections were stronger. This confirms the conclusion that the high-temperature phase is a solid solution of which elpasolite is an end member.

It is of interest to contrast Rb_2NaYF_6 and K_2NaYF_6 to K_2NaScF_6, previously grown and studied by Gabbe *et al.*[13] The latter system also crystallizes initially as a solid solution which decomposes upon cooling, but the boundary with the elpasolite is gradual rather than abrupt. Even the elpasolite, however, displays satellite x-ray reflections which decrease in intensity as a function of the amount of material grown. These additional reflections occur even though there is no optical evidence of a second phase, such as anisotropy or scattering. None of the other elpasolites display these extra reflections.

III. SPECTROSCOPY

Figure 2 is a diagram of the measurement system used for emission and excitation measurements. The sample was excited by a 1000-W xenon are lamp focused through a McPherson 0.3-m scanning monochromator. The monochromator housed a Bausch and Lomb 1200

TABLE I. Elpasolite lattice constants (Å).

Rb_2NaYF_6	8.869
K_2NaYF_6	8.72
Rb_2NaScF_6	8.60
K_2NaScF_6	8.482

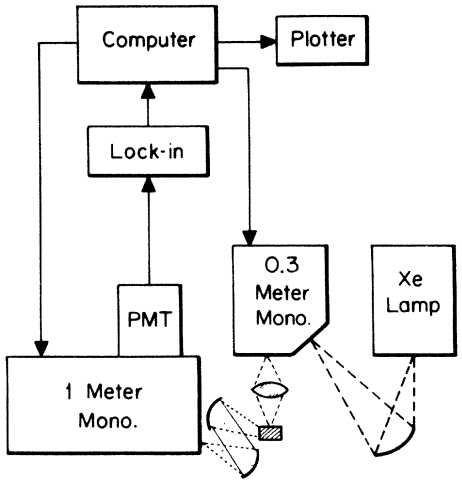

FIG. 2. Experimental apparatus for emission and excitation spectroscopy.

line/mm holographic grating blazed at 250 nm. The output beam from the monochromator was focused onto the sample with a quartz lens. The fluorescence from the sample was focused with reflective optics onto the entrance slit of a McPherson 1-m scanning monochromator. The monochromator housed a Bausch and Lomb 1200 line/mm ruled plane grating blazed at 200 nm. A tuning fork chopper was mounted at the entrance slit and chopped the fluorescence at 400 Hz, providing a reference signal for synchronous detection. For blue-green or near uv detection, the photomultiplier tube at the exit slit was a Hamamatsu R292. The detected signal was amplified by a PAR HR-8 lock-in amplifier.

The measurements were performed under computer control.[16] A Data General Nova 3 computer controlled the scanning of the monochromators, sampled the output of the lock in, performed data reduction and floppy-disk storage, and plotted the spectra on an HP 7523B plotter. The computer was used to correct the data for the spectral response of the detection system, or the spectrum of the excitation source. (This correction, called "normalization," was always done on a radiant power basis rather than on a photon-counting basis.) The computer was also used to calibrate the transmission wavelengths of the monochromators, and perform baseline subtraction and integration of spectra.

Emission spectra were measured by fixing the excitation wavelength and scanning the detection wavelength. To calibrate the spectral response of the detection system, an EPI-1363 tungsten filament lamp operated at 8.3 amps was used. Its radiation at a 50 cm distance was apertured and focused onto the entrance slit of the 1-m monochromator. Its emission spectrum was measured and then divided by lamp irradiance curves obtained at Epley for the same current and distance.

Excitation spectra were measured by fixing the detection wavelength and scanning the excitation wavelength. Normalization required the measurement of the spectrum of the exciting beam at the position of the sample. This was done by placing a $MgSO_4$-coated diffuse reflector at the sample position, focusing the illuminated area of the surface onto the entrance slit of the 1-m monochromator, and measuring the spectrum in the 200 to 350 nm range for various settings of the 0.3-m monochromator wavelength. This was done for settings ranging from 200 to 350 nm in 20 nm increments. Normalization of the spectra was achieved by reflecting deuterium lamp radiation off the diffuse reflector, measuring the spectrum, and dividing by NBS curves for the irradiance of the deuterium lamp.

Below 200 nm, transmission measurements were done on a vacuum-uv spectrometer designed by French and Jenssen.[17] The detectors for the reference and transmission paths were Hamamatsu R1080 photomultipliers.

Fluorescent decay measurements were done by exciting the sample by either a Molectron UV 12 pulsed nitrogen laser, or by a Molectron DL-II tunable dye laser pumped by the nitrogen laser. The fluorescent wavelength of interest was isolated using a Jarrell-Ash Model 82-410 monochromator, Corning glass filters, and/or interference filters. The fluorescence was detected with an RCA 6199, RCA 7102, Hamamatsu R292, or a dry-ice-cooled Amperex 150 CVP photomultiplier tube. A Tektronix 7623 oscilloscope was used as a wide-band amplifier and the vertical output signal from it was averaged and processed by an Analogic Data Precision D-6000 waveform analyzer.

Initially, all four elpasolites doped with cerium were spectroscopically evaluated. Emission, excitation, and absorption spectra were measured at room temperature. (An absorption spectrum was not obtained for K_2NaYF_6 because there were no clear single crystalline samples.) The samples used were Czochralski-grown Rb_2NaYF_6 doped with 1% Ce and grown from a stoichiometric melt, Czochralski-grown K_2NaScF_6 doped with 1% Ce, grown from a stoichiometric melt, Bridgman-grown Rb_2NaScF_6 with 1% Ce, and Bridgman-grown K_2NaYF_6 with 0.5% Ce.

Figure 3 shows excitation spectra and Fig. 4 shows the corresponding emission spectra for two emitting centers observed in Ce-doped Rb_2NaYF_6. There is a "blue site" giving rise to the emission band at 390 nm, and a "uv site" giving rise to the emission band at 340 nm. The behavior of Ce-doped K_2NaYF_6 is the same, except that the excitation and emission wavelengths are slightly dif-

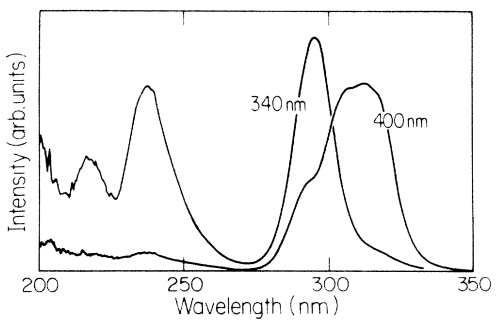

FIG. 3. Rb_2NaYF_6 excitation spectra.

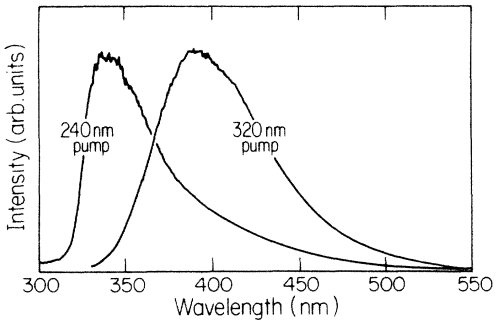

FIG. 4. Rb_2NaYF_6 emission spectra.

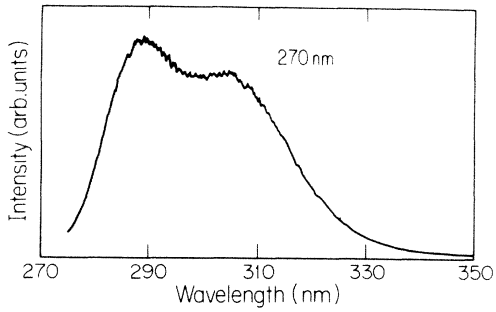

FIG. 6. K_2NaScF_6 emission spectrum.

ferent. Ce-doped Rb_2NaScF_6 displays only a "blue site" and K_2NaScF_6 displays only a "uv site." The excitation and emission spectra of the latter material are shown in Figs. 5 and 6, respectively. Of the four elpasolites, this is the only one in which the ground-state spin-orbit splitting of Ce^{3+} is clearly resolvable in the emission spectrum.

Fluorescent decay was measured for the 400 nm emission in Rb_2NaYF_6, Rb_2NaScF_6, and K_2NaYF_6. The pulsed nitrogen laser was used to excite the long wavelength tails of the 310—315 nm absorption bands and the decays were recorded on a Tektronix 7904 high-speed oscilloscope using an oscilloscope camera. The decays were exponential and in the 70—90 ns range.

The presence of two emitting centers in Rb_2NaYF_6 and K_2NaYF_6 raised the question of whether or not disordering in these hosts creates an alternate Y^{3+} site for trivalent rare earths. To test for this possibility, the Er-doped Rb_2NaYF_6 was grown. Er^{3+} is a very close match in ionic radius for Y^{3+}. Thus if some disordering occurs which gives rise to an alternate Y^{3+} site, Er^{3+} would serve as a spectroscopic "marker" for the alternate site. The $^4I_{15/2}$ to $^4I_{13/2}$ transitions in the absorption spectrum of Er^{3+} at 1.6 μm are magnetic-dipole allowed. Thus a low-temperature absorption spectrum identifies the number and position of the $^4I_{13/2}$ levels, and this can be compared to what is expected for the normal Y^{3+} site. Also, most of the other optical transitions of Er^{3+} are forbidden in inversion symmetry, leading to the absence of the pink coloration of the sample that accompanies these transitions when they are forced-electric-dipole allowed. This provides an easy visual test for the presence of a lower-symmetry site.

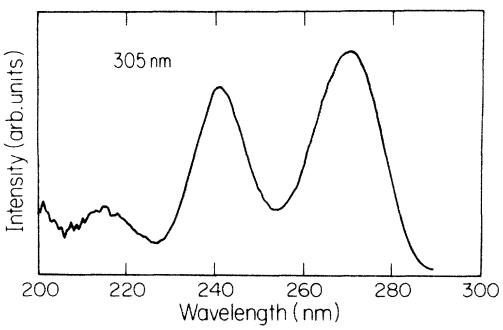

FIG. 5. K_2NaScF_6 excitation spectrum.

The feed for Bridgman-grown Er:Rb_2NaYF_6 was prepared with a 5% doping concentration of erbium, yet there was no pink coloration, either in the feed or the subsequently grown boules. Absorption spectra were measured on cut and polished slabs at room temperature, 77 and 8 K. Only three lines in the 1.6 μm region intensify as the sample is cooled, and their relative spectral positions closely match what is predicted by lattice sums run at Harry Diamond Laboratories[18] for the normal Y site, and the relative intensities of the three transitions also agree with the theoretically predicted pattern. The concentration was estimated to be 4.8% Er replacing Y, and no other transitions were observed which would indicate a second type of site. Thus, Y^{3+} is found only in its "normal" site, and Er^{3+} substitutes there with a high distribution coefficient.

Ce^{3+}, however, is 17% larger than Er^{3+}, and its incorporation might generate an optically active defect. To test this possibility, La-doped Rb_2NaYF_6 was grown. This sample showed no absorption band at 310 nm and none of the fluorescence or excitation bands present in the Ce-doped elpasolite. Therefore, both emitting centers arise from electronic transitions of the cerium complexes in the host.

The possibility that Ce^{4+} is incorporated into the crystal must also be tested. So, Ce-doped Rb_2NaYF_6 was grown in forming gas (95% argon, 5% hydrogen) to reduce the cerium to the trivalent state. Absorption spectra were measured on samples taken from boules grown in both argon and forming gas. The peak absorption coefficient of the 310 nm band is only 20% less in the reduced sample. The 310 nm band is therefore due to trivalent cerium. Emission from the second site is still observed in the reduced sample, and therefore also arises from trivalent cerium present in a much lower concentration.

Nd^{3+}-doped Rb_2NaYF_6 was grown to see if there are two sites for Nd^{3+}, since Nd^{3+} is almost as large as Ce^{3+}. A 1.7 cm thick slab was cut from the boule, and its absorption spectrum measured. The absorption was very weak ($\alpha = 0.02$ cm^{-1} at 570 nm). Again, the 310 nm band present in the cerium-doped samples was absent here.

The fluorescent decay was measured at 1.06 μm for various temperatures in the 4—600 K range. Two distinct emitting centers were observed, and the intensity of either

could be enhanced at the expense of the other by fine tuning the excitation wavelength. One center has a room temperature lifetime of less than 50 μs which increases to 130 μs at liquid-helium temperature. The other site has a 4.4 ms lifetime at room temperature which increases to 10.7 ms at 77 K and decreases again to 6 ms at 4 K. Above room temperature the lifetime shows a steady decrease to 2.85 ms at 568 K.

The emission spectra of the two sites was measured at 4 K by pumping the sample with a Rhodamine-6G cw dye laser. Again, the two sites could be separated by fine tuning the laser wavelength. The integrated intensity was a factor of 3 to 4 times greater for the short lifetime site. Since there are no efficient quenching paths known for the $^4F_{3/2}$ state, it is reasonable to assume that the lifetimes reflect the transition probabilities, and that the total intensity scales roughly with the product of the inverse lifetime and the concentration. By this criterion, the concentration of Nd^{3+} in the long lifetime site is about twenty times the concentration in the short lifetime site. Furthermore, the 4.4 ms room-temperature lifetime is one of the longest ever observed for Nd^{3+}, which indicates high symmetry.

The following conclusions are warranted for Ce-doped Rb_2NaYF_6.

(1) There are two sites, but the dominant site is the normal, high-symmetry one. About 95% of the cerium goes into this site, in the trivalent state, and gives rise to the absorption at 310 nm, and the 400 nm emission band.

(2) The other site seen in the excitation spectra is really cerium. It is more prominent in the sample grown by Czochralski pulling from a stoichiometric melt. In the Bridgman-grown samples (all grown from a Na-enriched melt) it is very weak. The splittings observed in the excitation spectra seem consistent with a roomy, low-symmetry site.

We can now propose a consistent explanation for the other elpasolites in the series. The spectrum of Ce^{3+} in the Sc^{3+} site should be similar in Rb_2NaScF_6 and K_2NaScF_6. However, they are drastically different, suggesting that a lower-symmetry site predominates in one of the two hosts. The absorption spectrum of K_2NaScF_6 shows four levels with relatively small splittings. The spectrum in Rb_2NaScF_6 shows a single band with at least an 18 000 cm^{-1} gap separating it from any others which might lie in the vacuum uv. Therefore, we conclude that Ce goes into the Sc site in Rb_2NaScF_6, and into a lower-symmetry site in K_2NaScF_6.

Similarly, Ce^{3+} should have similar spectra in the Y sites of Rb_2NaYF_6 and K_2NaYF_6. Therefore, the 315 nm band in the latter compound is ascribed to Ce^{3+} in the Y site.

Vacuum-uv transmission measurements were done on Ce:Rb_2NaYF_6, La:Rb_2NaYF_6, and Ce:Rb_2NaScF_6, in two overlapping spectral ranges, 110–210 nm and 170–270 nm. The long-wavelength scans were done with a uv quartz filter in the beam, which cuts off at 165 nm. This filters out the strong line emission of the hydrogen lamp, while passing a weaker, line-free continuum. A close match between the high-wavelength and low-wavelength scans was always obtained in the 170–210 nm region, indicating an acceptably low level of stray radiation through the monochromator.

Ce^{3+}-doped Rb_2NaYF_6 displays a weak, broad absorption band centered at 197 nm. Strong interband absorption occurs below 150 nm. La-doped Rb_2NaYF_6 completely lacks the 197 nm band but displays absorption near the band edge not present in the Ce-doped sample.

Ce^{3+}-doped Rb_2NaScF_6 displays a double-humped band with a stronger peak centered at 163 nm and a weaker one centered at 180 nm. The band edge of the host is also at 150 nm.

The broad emission of Ce^{3+} in the elpasolites is partially due to large crystal-field splittings of the $4f$ ground state. Theoretical calculations presented in Table IV place the highest $4f$ level at 5856 cm^{-1} above the ground state in Rb_2NaYF_6. $4f$-to-$4f$ absorption lines in the Ce-doped elpasolites were sought using the Cary 17D and the Beckman Acculab 10 Ir Spectrophotometer, but were too weak to be detected. Figure 7 shows an emission spectrum of Ce-doped Rb_2NaYF_6 at 4 K. Although the $4f$ splittings still cannot be resolved, there appears to be several heavily overlapping electronic transitions.

Although the second Ce^{3+} site in the elpasolites has not been identified, an educated guess is possible. When a helium-neon laser beam was directed through the samples of Rb_2NaYF_6 and Rb_2NaScF_6, scattering was seen only at the surfaces and not in the bulk. Therefore, the second site is not due to a precipitate. If a second phase is present, it is intergrown with the elpasolite; if such a second phase is not cubic, the intergrowth would have to be occurring on a very fine level with domains oriented in all three directions in order for the sample to appear optically isotropic. The satellite reflections in the diffraction pattern of K_2NaScF_6 are symptomatic of an intergrown second phase; K_2NaScF_6 is the only elpasolite displaying such reflections and is also the only elpasolite in which the second site is spectroscopically dominant. Therefore, one possible explanation is that the second phase houses a site with a much higher distribution coefficient than the normal site, but only in K_2NaScF_6 does the second phase occur in high enough concentrations to dominate over the normal site. Another explanation is that the second site is the Rb or K site in elpasolite since rare earths tend to go into sites of large size and high coordination number. Indeed, the absorption spectrum of Ce:K_2NaScF_6 looks

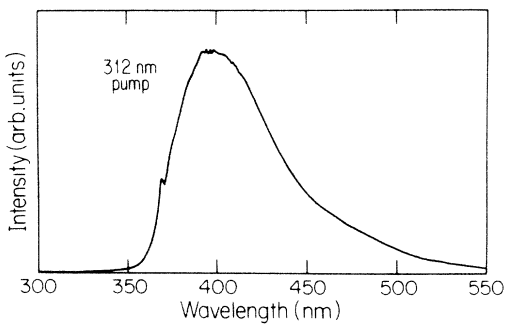

FIG. 7. Ce:Rb_2NaYF_6 emission spectrum at 4 K.

TABLE II. Experimental $5d$ energies (cm^{-1}) and lattice constants in elpasolites. Values of the $5d$-$4f$ centroid shift Δ are based on a free-ion centroid difference of 50000, and a $4f$ centroid which is 2000 cm^{-1} above the ground state in the elpasolites. (Estimated from Fig. 7).

Host	a (Å)	t_{2g}	e_g	$10Dq$	Δ
Rb_2NaYF_6	8.869	32500	50700	18200	−12000
K_2NaYF_6	8.72	31700			
Rb_2NaScF_6	8.60	32000	58800	26800	−9000

like that of a large, low-symmetry site. However, the fact that the second emitting center is observed in Rb_2NaYF_6 but not in Rb_2NaScF_6 is consistent with the hypothesis that disordering in the former compound assists in providing the necessary charge compensation.

IV. DISCUSSION

Table II lists the lattice constants, t and e levels, splittings and centroids for the elpasolites. The e level was not obtained for K_2NaYF_6 because the samples were polycrystalline and vuv transmission measurements were not feasible.

The t_{2g} and e_g energies in the table are taken to be the centroids of the absorption bands to the corresponding levels. In Rb_2NaYF_6 the centroid of the high-energy absorption band is estimated to be 197 nm, and in Rb_2NaScF_6 the centroid of the double-peaked vuv band is estimated to be 170 nm.

Before fitting the data to our phenomenological model, two observations should be made. First, the qualitative dependence of the levels on lattice constant is clearly characteristic of the intermediate covalency regime defined in conjunction with our model.[1] The $5d$ centroid rises as the lattice constant decreases, and the t_{2g} level is fairly insensitive to lattice constant, reaching a minimum value for K_2NaYF_6. Second, the increase in the splitting from Rb_2NaYF_6 to Rb_2NaScF_6 goes as a^{-12}, far greater than would be expected on the basis of an electrostatic model (i.e., a^{-5}). Both qualitatively and quantitatively, then, it is clear that covalency-overlap effects contribute significantly to crystal-field energies.

In formulating our phenomenological model[1] the nearest-neighbor distance was assumed to be a known quantity. In the undoped crystal this is found from x-ray analysis. The Y-F distance in Rb_2NaYF_6 is 2.1286 Å,[7] and, based on ionic radii, the Sc-F distance in Rb_2NaScF_6 should be close to 2.02 Å. Incorporation of the Ce^{3+} ion, however, will stretch the site. One way to estimate the actual impurity-ligand distance is to assume that only the nearest neighbors move, and that they are situated such that the Ce-Na distance is divided up according to the ratios of ionic radii. That is, the Ce-F distance is given by

$$R=(a/2)(r_{Ce}+r_F)/(r_{Ce}+2r_F+r_{Na}) .$$

This formula yields $R=2.2478$ Å for Rb_2NaYF_6 and $R=2.1795$ Å for Rb_2NaScF_6. In this work we will take R values roughly midway between this estimate and the values for the undistorted lattice:

$$R=2.20 \text{ Å for } Rb_2NaYF_6 ,$$

$$R=2.15 \text{ Å for } K_2NaYF_6 ,$$

$$R=2.10 \text{ Å for } Rb_2\ NaScF_6 .$$

We have five data points in Table II, and a six-parameter model [Eq. (23) of paper I]. However, the self-induced and lattice-induced dipolar splittings tend to cancel to within 2000 to 3000 cm^{-1}, so that the point-charge term dominates the electrostatic part of $10Dq$. Therefore no serious error is incurred by deleting the R^{-8} term altogether. This yields a set of five equations in five unknowns. Values of the exponential decay constant can be tried until consistency is obtained. The resulting parameters are

$$b=\tfrac{1}{15} \text{ Å} ,$$

$$C_1=8.76\times10^5 \text{ cm}^{-1} ,$$

$$A=2.55\times10^{17} \text{ cm}^{-1} ,$$

$$C_3=1.61\times10^6 \text{ cm}^{-1} ,$$

$$B=4.66\times10^{17} \text{ cm}^{-1} .$$

Use of these model parameters yields the following covalent contributions to the splittings and centroids. Rb_2NaYF_6:

$$10Dq(\text{cov})=1191 \text{ cm}^{-1} ,$$

$$\Delta(\text{cov})=2172 \text{ cm}^{-1} .$$

Rb_2NaScF_6:

$$10Dq(\text{cov})=5336 \text{ cm}^{-1} ,$$

$$\Delta(\text{cov})=9735 \text{ cm}^{-1} .$$

The covalent contribution to the splitting is 7% for Rb_2NaYF_6 the 20% for Rb_2NaScF_6. Our confidence in these results can be confirmed by calculating the values of effective ligand charge $-Z$ and polarizability α which would produce the above values of C_1 and C_3 in an *ab initio* calculation. Comparing (22) and (23) of paper I gives the correspondences

$$C_1=5Ze^2\langle r^4\rangle/3 ,$$

$$C_3=6\alpha e^2(\langle r^2\rangle_{5d}-\langle r^2\rangle_{4f}) .$$

Using Grossgut's[19] radial expectation values, we obtain $Z=1.19$ and $\alpha=1.86$ Å^3, which are very reasonable values.

TABLE III. $5d$ levels of Ce^{3+} (cm^{-1}). The numbers in parentheses indicate the energies of the emitting levels.

YLF		Rb_2NaYF_6	
b (x^2-y^2)	51 134	e_g	50 700
e $(zx+izy)$	49 367		
a (z^2)	41 828		
b (xy)	34 004	t_{2g}	32 500
Emission	(32 250)		(26 500)

V. ELPASOLITE AN $LiYF_4$: A COMPARISON

The Y^{3+} site in Rb_2NaYF_6 has six F^- neighbors at a distance of 2.1286 Å, forming a perfect octahedron. Y^{3+} in $LiYF_4$ (YLF) has eight F^- neighbors, at an average distance of 2.269 Å, forming an almost perfect dodecahedron.[20] The fluorescence spectra of Ce^{3+} in the two hosts are very different. Ce:YLF displays a double-humped band with peaks at 310 and 325 nm.[21] This is due to transitions to the two spin-orbit-split multiplets of the $4f$ ground state. Ce^{3+} in Rb_2NaYF_6 displays a single broad band peaking at 390 nm, with nearly twice the energy half-width as the double-humped band in YLF. Let us compare the energy levels of the two systems in order to elucidate the physical reasons for the spectroscopic differences. Table III shows the experimental $5d$ levels for Ce:YLF and Ce:Rb_2NaYF_6 derived from absorption or transmission spectra. The numbers in parentheses indicate the energies of the emitting levels, determined by inspecting the emission spectra and estimating the position of the band arising from the transition to the ground state. Table IV shows the $4f$ levels for the two systems, calculated by Morrison.[18]

Originally, we suspected that the long emission wavelength in Rb_2NaYF_6 is due to a large splitting produced by the octahedral coordination. That is, it was hypothesized that a dodecahedral coordination sphere is a closer approximation to a uniformly charged spherical shell than an octahedral coordination sphere. Purely on the basis of angular factors, the latter should produce a larger splitting. In particular, with octahedral coordination, the lobes of the e_g wave functions point directly at the ligands.

This hypothesis is not supported by the data, however. Inspection of Table III shoes that if the centroid and Stokes shift were the same for YLF and elpasolite, the emission in YLF would occur at an energy 3700 cm^{-1} less than the emission in elpasolite. A point-charge model explains the reason for this. Table V shows the $5d$ energy levels for a perfect octahedron and for a perfect dodecahedron of negative point charges for a bond distance of 2.2 Å. The $\langle r^2\rangle$ and $\langle r^4\rangle$ values of Grossgut[19] are used in the calculation, and the centroid is set to zero.

The hypothesis that a dodecahedral environment is "more isotropic" indeed seems to work for the levels that are destabilized by the ligands. The e_g state sustains 2.5 times the repulsion energy of the b_1 state. However, the levels which are most stabilized by the crystal field display the opposite pattern—the "more isotropic" environment produces a greater drop with respect to the centroid. In the case of the dodecahedron, the small repulsion energies for four of the five states require a large attraction energy for the remaining one (the b_2) in order to preserve the centroid.

The red-shifted emission in elpasolite as compared to YLF arises mainly from differences in the centroid and the Stokes shift. The $5d$ centroid is 5360 cm^{-1} lower in elpasolite than in YLF (measured with respect to the ground state). The Stokes shift is over 4200 cm^{-1} greater in elpasolite than in YLF. Both these factors favor longer-wavelength emission in elpasolite.

It is interesting to note that the $5d$-$4f$ centroid shift in YLF is about -6000 cm^{-1}, whereas it is at least twice as large in Rb_2NaYF_6. Yet the sum of e^2/R^6 over the ligands favors elpasolite by only 10%. This cannot be ascribed to a greater covalent contribution in YLF since YLF has a larger site and the metal-ligand overlap integrals are undoubtedly smaller than in elpasolite. Therefore, the effective fluoride polarizability is greater in elpasolite than in YLF. Crystal-field theory indeed predicts that in elpasolite the polarizability along the Ce-F bond axis is enhanced at the expense of the transverse polarizability. The F^- ion is colinear with its Ce^{3+} and Na^+ nearest neighbors. This stabilizes excited d states on the

TABLE IV. $4f$ energy levels of Ce^3 (cm^{-1}).

	YLF		Rb_2NaYF_6		
$^2F_{5/2}$	Γ_{56}	0			
	Γ_{78}	321	Γ_7	0	a_{2u}
	Γ_{56}	511			
			Γ_8	1941	
$^2F_{7/2}$	Γ_{78}	2378	Γ_7	2612	t_{2u}
	Γ_{56}	2439			
	Γ_{78}	2606	Γ_8	4876	
	Γ_{56}	3307	Γ_6	5856	t_{1u}

TABLE V. $5d$ splittings in a point-charge model (cm^{-1}).

Octahedron		Dodecahedron	
e_g	+8542	b_1	+3088
		e	+3066
		a_1	+457
t_{2g}	−5694	b_2	−9680

F^- ion which contribute to the polarizability along the bond axis, and destabilizes excited d states which contribute to the transverse polarizability. This enhances the $5d$ centroid drop because this effect is dominated by the axial polarizability. In YLF, the fluoride ion is closest to a Li^+ ion which lies in a direction nearly transverse to the Ce-F bond axis. Axial polarizability enhancement is not expected to occur to the same degree. Indeed, point-charge lattice sums[18] reveal that the attractive second-rank field on the fluoride ion along the Ce-F bond axis is roughly 3 times greater in elpasolite than in YLF.

Another important difference between YLF and Rb_2NaYF_6 is that the latter host produces much larger $4f$ splittings, as shown in Table IV. In YLF, the weak-field coupling scheme is appropriate, as there are two groups of closely spaced levels separated by a 2400 cm^{-1} gap, which is mostly the spin-orbit splitting.

In elpasolite, however, the strong field labeling is more appropriate, since the levels fall into three groups. The right-hand column of Table IV shows the cubic strong field labels. Although these splitting seem improbably large at first glance, they are in fact consistent with experimental evidence. The emission band in Fig. 7 can be fitted to overlapping bands with the indicated splittings. Furthermore, experimentally measured $4f$ levels[22] in $Cs_2NaCeCl_6$ display splittings as large as in YLF, although the nearest-neighbor distance in this elpasolite is over 2.7 Å.

At first, there seems to be a conflict between the behavior of the $5d$ splittings and the $4f$ splittings. Elpasolite $4f$ splittings are much greater than YLF $4f$ splittings, but the total $5d$ splittings are very similar; the total separation of the YLF b levels in Table III is 17 130 cm^{-1} compared to an 18 200 cm^{-1} splitting in elpasolite. The answer to the paradox is that the $5d$ splitting in YLF includes a large contribution from B_{20}, which has a large radial parameter. In a point-charge model for the $5d$ splittings, $\langle r^2\rangle/R^3$ is roughly twice as large as $\langle r^4\rangle/R^5$. In elpasolite, the $5d$ splitting must come entirely from the fourth-rank field, since B_{20} vanishes by symmetry. For the $4f$ electrons, however, the second-rank field is heavily shielded, and the competition is based on fourth- and sixth-rank fields. Thus the notion that elpasolite is "less isotropic" than YLF is confirmed by the $4f$ splittings. The dopant site in elpasolite is also tighter, as expected for a lower coordination number, and this also contributes to the strength of the crystal field.

Emissions to the three groups of levels in Table IV are not resolvable in the elpasolite spectra, even at liquid-helium temperature. In contrast, the 310 nm absorption band in elpasolite is quite narrow: two components separated by only 800 cm^{-1} are clearly resolvable. Jahn-Teller interactions are capable of softening certain vibrational modes in the emitting $5d$ state, and this would indeed produce emission bands which are much broader than the corresponding absorption bands. Further evidence of the Jahn-Teller effect is found in the 800 cm^{-1} splitting of the 310 nm absorption band. Indeed, the t_{2g} level should be split by the spin-orbit interaction into a Γ_8 and a Γ_7 level. Using the measured free-ion spin-orbit parameter, Morrison[23] determined that the Γ_7 should lie 1600 cm^{-1} above the Γ_8. Sugano and Shulman show that in Ni^{2+}, covalency reduces the spin-orbit parameter by only 3%. Therefore, the most plasible mechanism underlying the drastic reduction observed here is the Ham effect[24] quenching of the orbital angular momentum. If indeed the Jahn-Teller effect is operative, the associated distortion of the lattice makes a direct contribution to the Stokes shift.

VI. CONCLUSION

The qualitative dependence of the $5d$ levels on the lattice constant in the elpasolites clearly shows that covalency contributes significantly to the crystal-field interactions. Our numerical estimates of these contributions are consistent with this conclusion. In Rb_2NaScF_6, for example, covalency accounts for roughly 20% of the $5d$ splitting.

The results of this work suggest design rules for choosing a fluoride host which red shifts the $5d$-to-$4f$ emission of Ce^{3+}. First, the alternation of nearest-neighbor cations and anions along a straight line, including the substituted cation, is a desirable host property; it creates an anisotropic crystal field at the ligand which enhances the ligand polarizability along the dopand-ligand bond axis, which in turn brings down the $5d$ centroid. Second, a tight, strong-field site is desirable, and this usually occurs for low coordination numbers (4 or 6). Third, a high site symmetry has the potential advantage of enhancing the Stokes shift through a Jahn-Teller effect on the emitting $5d$ level.

ACKNOWLEDGMENTS

The authors gratefully acknowledge important contributions to this work by David Gabbe, Arthur Linz, Clyde Morrison, Richard Leavitt, Roger French, and Professor David Epstein. The figures were drawn by John Mara. Helpful insights were provided by Stanley Rotman, Professor David Adler, Professor Bernard Wuensch, Professor Harry Tuller, and Charles Naiman. Technical support was provided by Elaine Cook, Vladimir Belruss, Frank Payne, and Peter Kloumann. The work was supported partly by Sanders Associates, and the authors thank Tom Pollak and Evan Chicklis of Sanders for their support. Funding was also provided by the Army-Electronics Research and Development Command under Contract No. DAAK20-82-C-0135. Use was also made of Central Facilities sponsored by the National Science Foundation under Grant No. DMR81-19295.

*Present address: Lincoln Laboratory, Massachusetts Institute of Technology, Lexington, MA 02173.

[1]Brian F. Aull and Hans P. Jenssen, preceding paper, Phys. Rev. B 34, 6640 (1986).

[2]Richard K. Chang, U.S. Air Force Office of Scientific Research Report No. AFOSR-TR-82-0135, 1981 (unpublished).

[3]R. Roy, J. Am. Cer. Soc. 37, 581 (1954).

[4]J. G. Wurm, L. Gravel, and R. J. A. Potvin, J. Electrochem. Soc. **104**, 301 (1957).
[5]K. Knox and D. W. Mitchell, J. Inorg. Nucl. Chem. **21**, 253 (1961).
[6]G. Garton and B. M. Wanklyn, J. Cryst. Growth **1**, 49 (1967).
[7]S. Aleonard and C. Pouzet, J. Appl. Cryst. **1**, 113 (1968).
[8]P. J. Nassiff, T. W. Couch, W. E. Hatfield, and J. F. Villa, Inorg. Chem. **10**, 368 (1971).
[9]V. S. Schneider and R. Hoppe, Z. Anorg. Allg. Chem. **376**, 268 (1970).
[10]V. I. Siddiqi and R. Hoppe, Z. Anorg. Allg. Chem. **374**, 225 (1970).
[11]J. Chassaing, C. R. Acad. Sci. C **272**, 209 (1971).
[12]E. Bucher, H. J. Guggenheim, K. Andres, G. W. Hull, Jr., and A. S. Cooper, Phys. Rev. B **10**, 2945 (1974).
[13]D. R. Gabbe, B. F. Aull, and A. Linz, Proceedings of the Sixth American Conference on Crystal Growth, Atlantic City, 1984 (unpublished).
[14]A. Linz and D. R. Gabbe, in *Tunable Solid State Lasers,* edited by P. Hammerling, A. B. Budgor, and A. Pinto (Springer-Verlag, Berlin, 1985).
[15]Brian F. Aull Ph.D. dissertation, MIT Department of Electrical Engineering and Computer Science, 1985.
[16]Brian F. Aull (unpublished).
[17]Roger H. French, Ph.D. thesis, MIT Department of Materials Science and Engineering, 1985.
[18]Clyde Morrison (private communication).
[19]P. Grossgut, Ph.D. dissertation, Texas Christian University, 1971.
[20]C. Keller and H. Smutz, J. Inorg. Nucl. Chem. **27**, 900 (1965).
[21]D. J. Ehrlich, P. F. Moulton, and R. M. Osgood, Jr., Opt. Lett. **4**, 184 (1979).
[22]H.-D. Amberger, G. G. Rosenbauer, and R. D. Fischer, Mol. Phys. **32**, 1291 (1976).
[23]Clyde Morrison, Harry Diamond Laboratories (Adelphi, MD) Report No. HDL-TL-83-4, 1983 (unpublished).
[24]F. S. Ham, Phys. Rev. **138**, A1727 (1965).